Atmospheric
Chemistry
and Physics

The role of coarse aerosol particles as a sink of HNO₃ in wintertime pollution events in the Salt Lake Valley

Amy Hrdina[1,a], Jennifer G. Murphy[1], Anna Gannet Hallar[2], John C. Lin[2], Alexander Moravek[1,b], Ryan Bares[2], Ross C. Petersen[2,c], Alessandro Franchin[3,4], Ann M. Middlebrook[3], Lexie Goldberger[5,d], Ben H. Lee[4], Munkh Baasandorj[2], and Steven S. Brown[3]

[1]Department of Chemistry, University of Toronto, Toronto, ON, M5S 0A6, Canada
[2]Department of Atmospheric Sciences, University of Utah, Salt Lake City, UT 84112, USA
[3]Chemical Sciences Laboratory, NOAA Earth System Research Laboratories (ESRL), Boulder, CO 80305, USA
[4]Cooperative Institute for Research in Environmental Sciences (CIRES), University of Colorado, Boulder, CO 80309, USA
[5]Department of Atmospheric Sciences, University of Washington, Seattle, WA 98195, USA
[a]now at: Department of Civil and Environmental Engineering, Massachusetts Institute of Technology, Cambridge, MA 02139, USA
[b]now at: Department of Chemistry, York University, Toronto, ON, M3J 1P3, Canada
[c]now at: Department of Physical Geography and Ecosystem Science, Lund University, Lund, Sweden
[d]now at: Pacific Northwest National Laboratory, Richland, WA 99352, USA

Correspondence: Jennifer G. Murphy (jen.murphy@utoronto.ca)

Abstract. Wintertime ammonium nitrate (NH₄NO₃) pollution events burden urban mountain basins around the globe. In the Salt Lake Valley of Utah in the United States, such pollution events are often driven by the formation of persistent cold-air pools (PCAPs) that trap emissions near the surface for several consecutive days. As a result, secondary pollutants including fine particulate matter less than 2.5 μm in diameter (PM₂.₅), largely in the form of NH₄NO₃, build up during these events and lead to severe haze. As part of an extensive measurement campaign to understand the chemical processes underlying PM₂.₅ formation, the 2017 Utah Winter Fine Particulate Study, water-soluble trace gases and PM₂.₅ constituents were continuously monitored using the ambient ion monitoring ion chromatograph (AIM-IC) system at the University of Utah campus. Gas-phase NH₃, HNO₃, HCl, and SO₂ along with particulate NH₄⁺, Na⁺, K⁺, Mg²⁺, Ca²⁺, NO₃⁻, Cl⁻, and SO₄²⁻ were measured from 21 January to 21 February 2017. During the two PCAP events captured, the fine particulate matter was dominated by secondary NH₄NO₃. The comparison of total nitrate (HNO₃ + PM₂.₅ NO₃⁻) and total NH_x (NH₃ + PM₂.₅ NH₄⁺) showed NH_x was in excess during both pollution events. However, chemical

composition analysis of the snowpack during the first PCAP event revealed that the total concentration of deposited NO₃⁻ was nearly 3 times greater than that of deposited NH₄⁺. Daily snow composition measurements showed a strong correlation between NO₃⁻ and Ca²⁺ in the snowpack. The presence of non-volatile salts (Na⁺, Ca²⁺, and Mg²⁺), which are frequently associated with coarse-mode dust, was also detected in PM₂.₅ by the AIM-IC during the two PCAP events, accounting for roughly 5 % of total mass loading. The presence of a significant particle mass and surface area in the coarse mode during the first PCAP event was indicated by size-resolved particle measurements from an aerodynamic particle sizer. Taken together, these observations imply that atmospheric measurements of the gas-phase and fine-mode particle nitrate may not represent the total burden of nitrate in the atmosphere, implying a potentially significant role for uptake by coarse-mode dust. Using the NO₃⁻ : NH₄⁺ ratio observed in the snowpack to estimate the proportion of atmospheric nitrate present in the coarse mode, we estimate that the amount of secondary NH₄NO₃ could double in the absence of the coarse-mode sink. The underestimation of total nitrate indicates an incomplete account of the total oxidant

production during PCAP events. The ability of coarse particles to permanently remove HNO$_3$ and influence PM$_{2.5}$ formation is discussed using information about particle composition and size distribution.

---

1   Introduction

Episodes with high particulate matter (PM) pollution occur frequently in urban air basins across the globe during winter months when a stable boundary layer persists for multiple days, including in the mountain valleys in the western USA (Baasandorj et al., 2017; Bares et al., 2018; Green et al., 2015; Silcox et al., 2012; Whiteman et al., 2014), the Po Valley in Italy (Bernardoni et al., 2017; Vecchi et al., 2018), and the Sichuan (Tian et al., 2019) and Twin-Hu (Gao et al., 2019) basins in China. These mountain basins, including the Salt Lake Valley (SLV) in northern Utah, experience strong temperature inversions that develop into persistent cold-air pools (PCAPs), which suppress vertical mixing and trap emissions within a shallow boundary layer (Lareau et al., 2013; Whiteman et al., 2014). Under these conditions, mass loadings of fine particles smaller than 2.5 μm (PM$_{2.5}$) often reach values of 60–80 μg m^{-3} in the western USA, which are far above the US National Ambient Air Quality Standard (35 μg m^{-3}, 24 h average) (Lareau et al., 2013; Silcox et al., 2012; Whiteman et al., 2014). Along with environmental impacts such as haze and localized deposition, mass loadings of PM$_{2.5}$ that exceed this standard have been associated with increased risk of mortality, especially cardiopulmonary or cardiovascular disease mortality (Pope et al., 2003, 2017). However, despite significant societal concerns about the impact on human health from these PM$_{2.5}$ pollution episodes and their common occurrence around the world, the major chemical processes that drive PM formation in these regions are still uncertain.

Several studies conducted in northern Utah have shown that PM$_{2.5}$ during these PCAP episodes is predominantly composed of ammonium nitrate (NH$_4$NO$_3$), accounting for roughly 60 %–80 % of the total dry particle mass (Baasandorj et al., 2017; Franchin et al., 2018; Hansen et al., 2013; Kelly et al., 2013; Kuprov et al., 2014; Long et al., 2002, 2003; Mangelson et al., 1997). NH$_4$NO$_3$ formation is thermodynamically favorable under conditions with low temperatures and high relative humidity based on equilibrium partitioning with gas-phase ammonia (NH$_3$) and nitric acid (HNO$_3$) (Mozurkewich, 1993; Nowak et al., 2010; Seinfeld and Pandis, 2006), illustrated in the right-hand portion of Fig. 1.

NH$_3$ emissions are often associated with agricultural activities and waste disposal; however, in recent years automotive emissions and industrial processes have become increasingly important sources in urban areas (Behera et al., 2013; Bishop et al., 2010, 2016; Livingston et al., 2009; Nowak et al., 2012; Roth et al., 2019; Suarez-Bertoa et al.,

2014; Sun et al., 2017). In contrast, HNO$_3$ is formed in the atmosphere and is a major sink of nitrogen oxides, which are emitted primarily through fossil fuel combustion. The two dominant mechanisms highlighted in Fig. 1 that lead to HNO$_3$ occur either (1) from oxidation of NO$_2$ via reaction with OH (in orange), which is photochemically driven during the day, or (2) through heterogenous uptake of N$_2$O$_5$ (in black), which typically occurs at night. Gas-phase HNO$_3$ and NH$_3$ and particulate NH$_4$NO$_3$ are removed from the atmosphere through dry and wet deposition under typical atmospheric conditions. However, under PCAP conditions, the stably stratified boundary layer reduces convective mixing, which in turn allows pollutants to accumulate. In addition, HNO$_3$ can also be lost through heterogenous reaction with dust and sea salt components, such as CaCO$_3$ and NaCl (Beichert and Finlayson-Pitts, 1996; Dasgupta et al., 2007; Fenter et al., 1994; Liu et al., 2008a). When the loss of HNO$_3$ to deposition is suppressed under PCAP conditions, the loss to reactive uptake to airborne dust and sea salt can potentially become more important.

To formulate effective control strategies that reduce wintertime PM$_{2.5}$ in northern Utah, measurement campaigns have been conducted to improve our understanding of fine particulate formation during these PCAP episodes (Baasandorj et al., 2017; Bares et al., 2018; Hansen et al., 2010; Kelly et al., 2013; Kuprov et al., 2014; Lareau et al., 2013; Malek et al., 2006; Mangelson et al., 1997; Silcox et al., 2012; Whiteman et al., 2014). Several analyses of the PM buildup in cold-air pool events in the SLV have been published, all based on measurements from one or several ground sites (Baasandorj et al., 2017; Kuprov et al., 2014; Long et al., 2003; Silcox et al., 2012). Long-term PM$_{2.5}$ composition measurements in the SLV are made using filter samples (Kelly et al., 2013; Kuprov et al., 2014; Long et al., 2003; Mangelson et al., 1997; Silcox et al., 2012; Whiteman et al., 2014), with PM$_{2.5}$ speciation carried out on filter extracts in accordance with the US Environmental Protection Agency (EPA) Speciation Trends Network (STN) protocol. Kuprov et al. (2014) were the first to report the gas and PM$_{2.5}$ composition during pollution events in northern Utah using an ambient ion monitoring ion chromatograph (AIM-IC) system; however, this study only measured anionic species, providing HNO$_3$ and particle nitrate (pNO$_3^-$) concentrations at an hourly resolution. Ambient NH$_3$ concentrations were monitored using a chemiluminescence-based NH$_3$ analyzer, but particulate ammonium (pNH$_4^+$) had to be inferred based on the assumption that both pNO$_3^-$ and particulate sulfate (pSO$_4^{2-}$) were in the form of their respective ammonium salts. Particle mass fractions of crustal and carbonaceous material in PM$_{2.5}$ were calculated on 24 h average measurements of Al, Si, and elemental and organic carbon in fine particles from the NCore program (US EPA, 2010).

Recent research in the SLV has focused on determining whether ammonium nitrate mass loading is most sensitive
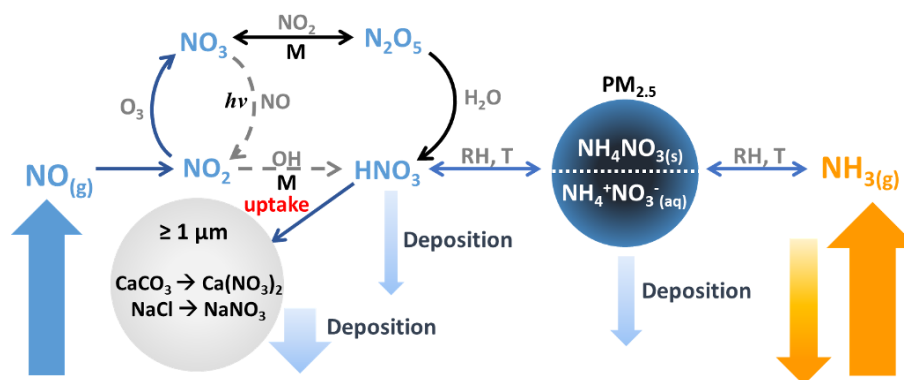
Figure 1. Processes influencing the concentrations of NH_3, NO_x, HNO_3, and NH_4NO_3. Pathways that occur during the day are shown in dashed grey arrows, while pathways that occur during the night are shown in black. The rate of uptake of HNO_3 to coarse particles, $\geq PM_1$, composed of $CaCO_3$ and/or NaCl is unknown.

to reductions in NH_3 or HNO_3 to inform $PM_{2.5}$ reduction strategies (Kuprov et al., 2014). Baasandorj et al. (2017) recently proposed that $PM_{2.5}$ forms overnight in the upper layers of the PCAP and mixes down to the surface, enhancing the total $PM_{2.5}$ loading experienced in the SLV. This explanation of stratified particulate nitrate chemistry throughout PCAP events suggests a complex coupling of a HNO_3-limited surface layer with a NH_3-limited elevated layer (Baasandorj et al., 2017). Aircraft measurements during the 2017 Utah Winter Fine Particulate Study (UWFPS) provided the first detailed vertically resolved chemical composition of these PCAP episodes in the SLV. Analysis presented in McDuffie et al. (2019) confirms that the formation of NH_4NO_3 during these pollution events is largely limited by HNO_3 but with more frequent periods approaching NH_3-limited conditions in the upper boundary layer over time (McDuffie et al., 2019). Regimes of both NH_3-limited and HNO_3-limited conditions are also consistent with an aerosol thermodynamic model sensitivity study of the same data by Franchin et al. (2018), who found simulations of non-refractory PM_1 mass were sensitive to reductions in both total ammonium and total nitrate (Franchin et al., 2018). Box model studies of the odd oxygen budget during UWFPS by Womack et al. (2019) assumed that NH_4NO_3 formation during PCAP episodes is HNO_3-limited, and found full episodes tend to be NO_x-saturated. In conditions where pNO_3^- production is HNO_3-limited, it is often assumed that reduction in NO_x would directly lead to reductions in HNO_3. However, Womack et al. (2019) showed the production of HNO_3, and therefore, NH_4NO_3 formation, is sensitive to changes in VOC concentrations emphasizing the complexity of chemical processes involved in PM formation under these conditions.

The balance of factors influencing HNO_3 formation are still being understood. Modelling results from both McDuffie et al. (2019) and Womack et al. (2019) predict that up to $\sim 50\%$ of HNO_3 production is from the heterogeneous N_2O_5

pathway in the residual layer. This is in line with ground-based measurements of N_2O_5 by Baasandorj et al. (2017) highlighting the importance of nighttime pathway (Baasandorj et al., 2017). Less attention has been paid to the possibility that alternate sinks for HNO_3 may also significantly limit the amount of nitrate that can contribute to $PM_{2.5}$ formation.

Here, results are presented from ground site observations in Salt Lake City from a moderately elevated site at the edge of the SLV during the UWFPS campaign in January and February 2017. Atmospheric concentrations of inorganic trace gases and water-soluble $PM_{2.5}$ constituents were measured by an AIM-IC, equipped with both cation and anion ion chromatographs. During PCAP episodes, we observed the formation and build-up of NH_4NO_3 over several days. Between the hours of 08:00 and 18:00 mountain standard time (MST) on several PCAP days, we also observed the presence of elevated levels of non-volatile cations in $PM_{2.5}$. To investigate the role of mineral–coarse-mode aerosols in limiting the availability of HNO_3 during these events, the final section presents estimates of HNO_3 lifetime against reactive uptake onto mineral–coarse-mode dust based on aerodynamic particle sizer (APS) data and estimates of the total nitrate budget using the chemical composition of the snowpack measured during UWFPS.

2 Methods

2.1 Site description

The SLV ($1300\,km^2$) is a mountain basin in northern Utah surrounded by steep mountain ranges with the Great Salt Lake sitting to the northwest. The Wasatch Mountains (peak at 3636 m a.s.l.) span the entire eastern border of the valley with the Oquirrh Mountains (peak at 3235 m a.s.l.) to the west. There is a narrow passage in the southern Traverse Range (1878 m a.s.l.) that creates a small opening into

the Utah Valley. Salt Lake City sits at the base of the valley (1288 m a.s.l.), making a vast elevation difference between the metropolis and the surrounding mountains. Measurements were conducted from the rooftop of the William Brown Building 33 m above ground level at the University of Utah (UU) located 40°45′58.7″ N, 111°50′51.6″ W, in Salt Lake City. The UU site is located 155 m above the valley floor along the northeast sidewall of the SLV. The site is impacted by local traffic that enters the university on the north side of campus.

2.2 Instrumentation

Hourly averages of PM$_{2.5}$ chemical composition and gas-phase precursors were measured using an online continuous AIM-IC instrument (Model 9000D, URG Corp, Chapel Hill, NC). Briefly, gases and particles are sampled from the same airflow by passing through a short inlet with elements for size selection (PM$_{2.5}$ impactor), gas collection (wet parallel plate denuder), and particle capture (saturation chamber) at a flow rate of 3 L min^{-1}. Aqueous solutions containing analytes originally in the gas and particle phases are separately transferred through 22 m inlet lines into 5 mL glass syringes that are subsequently analyzed by ion chromatographs (ICs) following hour-long collection periods. More in-depth details about the AIM-IC system, including important adaptations from the standard commercial system, can be found in Markovic et al. (2012). During the UWFPS campaign, the components of the inlet assembly were housed in a small weatherproof box 2 m above the roof of the UU site and the IC systems were housed in a laboratory below. Standard calibrations of the ICs were performed offline using mixed ion standard solutions before and after the measurement period. Charged species (Na$^+$, NH$_4^+$, K$^+$, Mg^{2+}, Ca^{2+}, NH$_3$, amines, Cl$^-$, NO$_2^-$, NO$_3^-$, and SO$_4^{2-}$) were measured using a Dionex ICS-2000 equipped with concentrator columns (TCC-ULP1 and TAC-ULP1), guard columns (CG17 and AG19), and 4 mm analytical columns (CS17 and AS19). Gradient elution methods, using methanesulfonic acid (MSA) and potassium hydroxide (KOH), were carried out using electrolytically regenerated suppressors to reduce the influence of the eluent in the conductivity detection. Carbonate salts are never quantified in the anion IC due to the natural presence of carbonate in the distilled deionized water reservoir that sustains the IC systems. Background measurements of the entire AIM-IC system were conducted by overflowing the sampling inlet using high-purity zero air to determine the method zero and detection limits of each species. The limits of detection (LODs), based on 3σ of the background, for trace gases were found to be 150, 20, 40, and 10 ppt for NH$_3$, HCl, HNO$_3$, and SO$_2$, respectively. The LODs for PM$_{2.5}$ chemical constituents were 0.2, 0.1, 0.1, 0.04, and 0.4 µg m^{-3}, for pNH$_4^+$, pNa$^+$, pK$^+$, pMg^{2+}, and pCa^{2+} and 0.03, 0.03, and 0.01 µg m^{-3} for pCl$^-$, pNO$_3^-$, and pSO$_4^{2-}$. Traces gases and PM$_{2.5}$ constituents measured

as cations are reported from 21 January to 21 February 2017. Due to technical difficulties, anionic constituents measured from 21 January to 8 February were compromised. Therefore, PM$_{2.5}$ anionic components are only reported from 13 to 21 February and the trace gases measured as anions during the former period may be less reliable.

Continuous measurements of total PM$_{2.5}$ mass concentrations were also captured at the site using the Filter Dynamics Measurement System (FDMS) with a tapered element oscillating microbalance (TEOM) ambient particulate monitor (FDMS TEOM 1400ab, Thermo Fisher Scientific) provided by the Utah Division of Air Quality (UDAQ). Ambient air was sampled at ∼ 1.5 m above the roof through a ∼ 7 m long 1/4″ o.d. PFA line with a volumetric flow rate of 20 L min^{-1}. A custom-made inertial PM impactor was connected to the entrance of the sampling inlet to remove coarse PM and water from the sample flow. A critical orifice was installed downstream of the PM impactor to restrict the sample flow, maintaining a pressure below 200 mbar. The air sample was sent through an additional filter to remove particles larger than 2.5 µm. An aerodynamic particle sizer (APS; TSI Inc, Model 3321) was operated from 26 January to 10 February to size and detect particles with an aerodynamic diameter of between 0.54 and 19.81 µm based on the time of flight of the particle between two (633 nm) He-Ne lasers. This instrument was attached to an aerosol inlet that included a 2.54 cm diameter stainless-steel tube connected to a stainless-steel rain cap with approximately a 10 cm diameter. Aerosol mass was calculated using the Aerosol Instrument Manager (AIM) software for the APS Model 3321. The particle density used for calculating the aerosol mass concentration was 1.0 g cm^{-3}, and particles were assumed to be spherical. The APS was attached to this inlet system via a custom-made stainless-steel pickoff. To improve aerosol transmission through the inlet, an external pump was attached to the system. The pump pulled at approximately 7.2 L min^{-1}. The calculated transmission shows a 50 % cutoff at approximately 7 µm for this inlet system (Skiles et al., 2018).

2.3 Snow sampling and analysis

The inorganic chemical composition (Na$^+$, NH$_4^+$, K$^+$, Mg^{2+}, Ca^{2+}, NH$_3$, Cl$^-$, NO$_2^-$, NO$_3^-$, and SO$_4^{2-}$) of the snowpack was monitored throughout the campaign during periods of snow cover. The snowpack composition and depth were measured daily within a 2 m radius around the AIM-IC inlet atop UU using a clean graduated 5 cm diameter beveled snow corer. Samples were collected in triplicate along with a field blank to account for any contamination during sampling. Collected samples were melted in sealed containers. The resulting snowmelt solution was measured for total melt volume and pH (Hach sensION+ PH1 Portable pH Meter). Snowmelt samples were then filtered through 0.25 µm PTFE filters (Whatman, VWR International) before analysis utilizing ion chromatography.

2.4 Aerosol thermodynamic modelling using ISORROPIA

Thermodynamic modelling was used to examine the expected gas and particle partitioning of semi-volatile constituents based on the local meteorological conditions and the observed concentrations of gas and particle constituents. These models carry out bulk calculations to estimate the gas-phase and particle-phase composition of inorganic species, in which all particles are assumed to have the same chemical composition. To examine how the presence of non-volatile particle components observed during this period may affect nitrate partitioning, ISORROPIA v2.1 (Nenes et al., 1998; Fountoukis and Nenes, 2007) was used. Model calculations were run in forward mode, with observed total ammonia ($NH_3 + pNH_4^+$), particulate sulfate (pSO_4^{2-}), total nitrate ($HNO_3 + pNO_3^-$), total chloride ($HCl + pCl^-$), and non-volatile particulate species (pK^+, pNa^+, pCa^{2+}, and pMg^{2+}), along with ambient relative humidity and temperature, as inputs. Model runs were conducted using the metastable state option, which prevents solid formation by forcing all particulate components to remain in an aqueous state.

3 Results and discussion

3.1 Trace gas and $PM_{2.5}$ composition in the Salt Lake Valley

The AIM-IC measurement period included two PCAP pollution episodes, 27 January to 3 February 2017 (episode 1) and 13 to 17 February 2017 (episode 2), defined by the meteorological conditions that stabilize the boundary layer and by the total observed $PM_{2.5}$ mass, separated by a relatively clean period from 5 to 12 February 2017. The PCAP episodes can be clearly seen in the build-up of $PM_{2.5}$ mass and the inorganic constituents measured by the AIM-IC as shown in Fig. 2. Pollution periods with a total 24 h average $PM_{2.5}$ mass $> 17.5 \, \mu g \, m^{-3}$ are deemed PCAP periods, while periods with a 24 h average $PM_{2.5}$ mass $\leq 2 \, \mu g \, m^{-3}$ are considered clean periods, as previously defined by Whiteman et al. (2014). The pollution period from 27 January to 3 February 2017 (episode 1) was the most persistent and severe during the UWFPS measurement campaign.

Both pollution events are marked in Fig. 2, while the full suite of inorganic gases and $PM_{2.5}$ components was measured by the AIM-IC only from 8 to 19 February 2017. The increase in total $PM_{2.5}$ mass at the onset of episode 1 on 27 January coincides with a rise in pNH_4^+, seen in Fig. 2a, while there is an initial drop in ambient NH_3 concentration before it plateaus at a mixing ratio of ~ 1 ppb as the PCAP progresses. The HNO_3 and pNO_3 data, depicted in Fig. 2b for the second pollution event, confirm the major water-soluble component of $PM_{2.5}$ in the SLV is NH_4NO_3, as

previously reported (Hansen et al., 2010; Kelly et al., 2013; Kuprov et al., 2014; Long et al., 2003). Compared to the pCl^- and pSO_4^{2-} mass loadings measured during that event, Fig. 2b shows the total mass of pNO_3^- is an order of magnitude larger. Particularly at midday, the majority of the $PM_{2.5}$ mass is NH_4NO_3. It is important to note the organic fraction of $PM_{2.5}$ was not measured by the AIM-IC. Based on TEOM total mass and AIM-IC-measured mass fractions, the AIM-IC captured 75 % of the total $PM_{2.5}$ mass.

The distinction between PCAP episodes 1 and 2 is important to note because the stability of the cold-air pool and its persistence influences the intensity of $PM_{2.5}$ build-up in the SLV. Episode 1 was the most severe, persisting for 9 d and allowing $PM_{2.5}$ daily averages to reach the highest observed through the measurement period, a maximum hourly average of $60 \, \mu g \, m^{-3}$. The episode occurred a few days after a storm deposited roughly 22 cm of snow across the SLV and Wasatch front. Ambient temperatures remained below freezing, between 263 and 273 K, sustaining the snowpack throughout the event. This in turn increased the surface albedo, limiting the strength of convection that can disrupt the stable boundary layer (Whiteman et al., 2014). Winds during this episode were light, averaging $1 \, m \, s^{-1}$, with gusts under $7 \, m \, s^{-1}$ during the most stable and calm cold pool period from 31 January to 2 February.

The second PCAP observed during the campaign was much shorter-lived with moderate cold pool conditions only present from 13 through 17 February. This episode was distinctly different than episode 1, having no snow cover and much warmer conditions, with temperatures ranging from 270 to 284 K. The winter snowpack in the surrounding mountain range showed signs of spring melt, which extended the surface area of exposed ground. Winds were slightly stronger, averaging $1.6 \, m \, s^{-1}$ with stronger gusts averaging around $8 \, m \, s^{-1}$ caused by stronger convection. The hourly $PM_{2.5}$ average at the UU site peaked at $28 \, \mu g \, m^{-3}$, and elevated PM levels only persisted for 2 to 3 full days, so the intensity and duration of episode 2 was about half that of episode 1.

The presence of non-volatile cations (pCa^{2+}, pMg^{2+}, pK^+, and pNa^+), seen in Fig. 2c, was also observed during PCAP events. Of all the non-volatile cations observed, only potassium increases with the same pattern as the increase in pNH_4^+ and total $PM_{2.5}$ mass measured by the TEOM. Potassium salts are often found in primary aerosols formed from biomass or biofuel burning (Pósfai et al., 2003; Rissler et al., 2006). Wood burning is still a commonly used source of heat during the winter months in the SLV and could be the source of pK^+ observed during the severe PCAP episode 1. Aerosol mass spectrometer (AMS) data from Franchin et al. (2018) showed traces of levoglucosan, a known marker for wood combustion, during the pollution episode. However, levoglucosan was typically measured at close to background values. Overall, the data reported from AMS measurements indicated the organic material from wood combustion is not
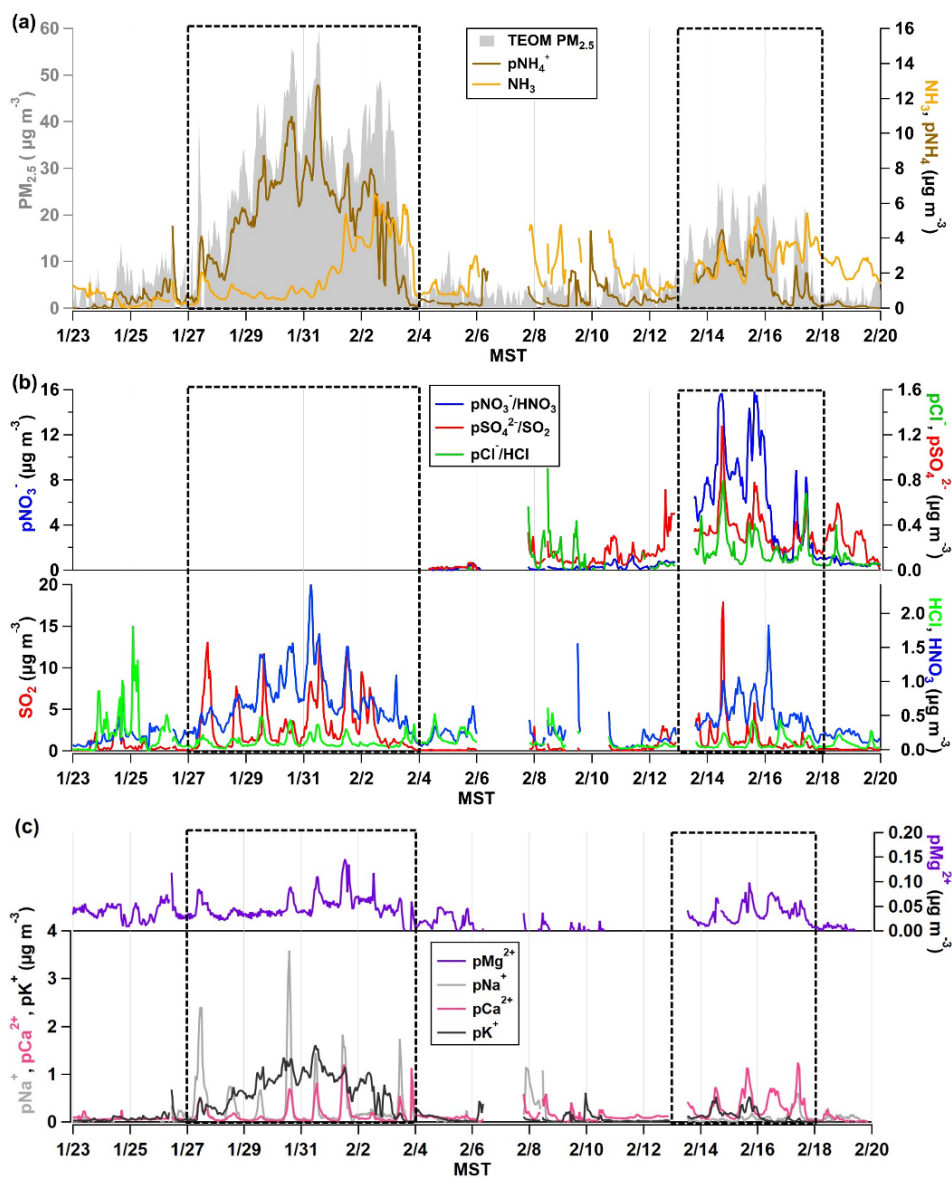
Figure 2. (a) The time series of NH_3 and pNH_4^+ observed by the AIM-IC and total $PM_{2.5}$ mass loading ($\mu g\,m^{-3}$) measured by the TEOM from 23 January to 19 February 2017. **(b)** The AIM-IC observations of inorganic gases HCl, HNO_3, and SO_2 and $PM_{2.5}$ components pCl^-, pNO_2^-, pNO_3^-, and pSO_4^{2-} present in $PM_{2.5}$. **(c)** The AIM-IC observations of the non-volatile inorganic cations pNa^+, pK^+, pMg^{2+}, and pCa^{2+} measured in $PM_{2.5}$ for the entire campaign period. The two PCAP pollution episodes captured during the campaign are emphasized by the dotted black line. Time is expressed in mountain standard time (MST).

a dominant mass fraction on the regional scale (Franchin et al., 2018). Recent radiocarbon analysis from ground sites in the SLV indicates that fossil fuels were the dominant sources of carbonaceous aerosols during winter, contributing to 88 % (80 % to 98 %) of the black carbon in aerosols and 58 % (48 % to 69 %) of the organic carbon in aerosols (Mouteva et al., 2017). Similarly, the AIM-IC data also suggest that pK^+ salts generally compose a small fraction of the total $PM_{2.5}$ mass.

The alkali and alkaline metal components pCa^{2+}, pMg^{2+} and pNa^+ are commonly found in larger primary particles often emitted from the lofting of mineral dust and salts. These species are often found in mineral aerosols, which typically range from 0.1 to more than 10 μm, partially contributing to $PM_{2.5}$ (Zender, 2003). The coarse-mode fraction of these primary particles, with diameters greater than 2.5 μm, has sufficiently large settling velocities that the particles have much shorter lifetimes in the atmosphere compared to $PM_{2.5}$. If the non-volatile cations observed in $PM_{2.5}$ are present in

the largest fine particles, then their lifetime in the atmosphere is considerably shorter than NH$_4$NO$_3$ found in the accumulation mode. This may be the explanation for the more pronounced diel pattern of pCa^{2+}, pMg^{2+}, and pNa$^+$ during the PCAP periods. It is also possible that because vertical mixing is suppressed during PCAP episodes, the UU site is in contact with air from the mineral dust source region to a measurable degree only at midday. During the clean periods, the concentrations of these ions measured by the AIM-IC are very close to their respective detection limits. pNa$^+$, pCa^{2+} and pMg^{2+} PM$_{2.5}$ components peak at midday during pollution events, suggesting similar and/or co-located sources. Concentrations of pMg^{2+}, which is an effective tracer for mineral dust along with pCa^{2+} (Maxwell-Meier et al., 2004), are present throughout the entire measurement period, averaging 0.02 µg m^{-3} and reaching a maximum of 0.15 µg m^{-3}. It is known that sea salt is the most common source of pNa$^+$, so examining the Ca-to-Na ratios can suggest the predominant source. Particularly for the SLV region, the Great Salt Lake can also be a source of sea salt. In PCAP episode 1, Ca-to-Na ratios were below 1, suggesting the presence of sea salts. In contrast, in episode 2 ratios of Ca-to-Na were above 1, suggesting the sources of these particulate components differ between the two PCAP periods. Due to the heavy snowfall during episode 1, road salt was continuously applied to all major roads and walkways throughout the UU campus, which may act as a local source of Na salts during periods of heavy traffic. The lack of snow cover during the latter episode and higher temperatures may suggest some influence of mineral dust from the surrounding ground surface areas, where sediments and weathered minerals are often Ca-rich (Chesselet et al., 1972; Kassomenos et al., 2012; Kuo et al., 2005). Recent studies have found the Great Salt Lake is quickly receding, suggesting the exposed the lake bed could act as a source of dust and sea salt (Hahnenberger and Nicoll, 2012; Skiles et al., 2018; Wurtsbaugh et al., 2017). However, the bulk PM$_{2.5}$ chemical composition measured by the AIM-IC is not detailed enough to unambiguously identify the source of non-volatile cations observed during PCAP events.

3.2 Estimating HNO$_3$ loss to coarse-mode particles

Gas-phase HNO$_3$ exists in equilibrium with semi-volatile nitrate in PM$_{2.5}$, and the extent of gas-to-particle partitioning depends on temperature, relative humidity, and NH$_3$, via the formation of NH$_4$NO$_{3(s)}$ in dry particles or its influence on particle acidity in deliquesced particles. At the same time, HNO$_3$ may undergo net uptake by primary particles when it reacts with their constituents, for example CaCO$_3$ or NaCl, to form non-volatile nitrate salts. The rate of HNO$_3$ loss can be impacted by the composition of the reactive salt and the reactive surface area available (Seinfeld and Pandis, 2006). During the two PCAP episodes, we observed elevated midday concentrations of pNa$^+$, pCa^{2+}, and pMg^{2+} in PM$_{2.5}$ using the AIM-IC.

3.2.1 Inferences from aerodynamic particle sizing

Coarse-mode particles (diameters > 2.5 µm) were not speciated during the UWFPS campaign. There are very few reports of coarse-mode nitrate in winter conditions that could offer an approximation of how much HNO$_3$ may have been taken up by coarse-mode particles in the SLV. The study of Hansen et al. (2010) is the only one commenting on coarse-mode nitrate in northern Utah region, in Lindon, ∼ 50 km located south of the SLV, during January to February 2007. The authors observed high mass loadings, up to 80 µg m^{-3} of coarse aerosols (PM$_{10}$–PM$_{2.5}$), during PCAP events, based on measurements from two GRIMM optical particle counters (Hansen et al., 2010). The authors did not report any quantification of the chemical components of the coarse aerosols collected by integrated filter samples, although they commented that the nitrate levels were relatively low.

To obtain information about the coarse-mode loadings during PCAP events in UWFPS, APS data collected during the pollution episode from 28 January to 3 February are displayed in Fig. 3. The particle size bins are colored by mass normalized to the size bin (dM/d log Dp), clearly showing elevated midday burdens of coarse-mode particles, which become more pronounced during the intensive cold-air pool period from 30 January to 2 February 2017. This is consistent with the midday increases in coarse-mode mass observed across the SLV, shown in Fig. 4. The coarse fraction of PM$_{10}$ measured at Hawthorne Elementary (the air quality regulatory site at the base of the SLV operated by UDAQ) shows a similar trend to the APS mass loading of PM$_{10}$–PM$_{2.5}$ observed at UU. In contrast, the Rose Park site (another UDAQ site), which is close to Great Salt Lake, exhibits moderate increases in coarse-mode mass compared to UU and Hawthorne. This difference is more evident during the calmest period of the pollution event, when the lowest wind speeds were observed, which suggests the sources of coarse particles are highly localized during PCAP events. An analysis of coarse particles by Li et al. (2013) found only moderate correlation between PM$_{10-2.5}$ mass loadings and wind speed at several sites across the USA (Li et al., 2013).

The time series of the total surface area of PM larger than 2.5 µm in µm^2 cm^{-3} (Fig. 3) shows the available coarse-mode surface area exceeds 1500 µm^2 cm^{-3} for several hours on each of the 3 most severe pollution days, 30 January to 1 February 2017. For comparison, the total surface area of the fine-mode particles is also shown, which is roughly 3 times the maximum surface area of the coarse fraction but with less diurnal variability. However, the fine-mode aerosol nitrate is assumed to be in equilibrium with gas-phase HNO$_3$, in contrast to the coarse-mode surface area, which could be viewed as a reactive sink allowing net uptake. The midday increases in coarse-particle surface area, therefore, could represent an important permanent sink for HNO$_3$ if the particles are composed of reactive salts such as CaCO$_3$ or NaCl.
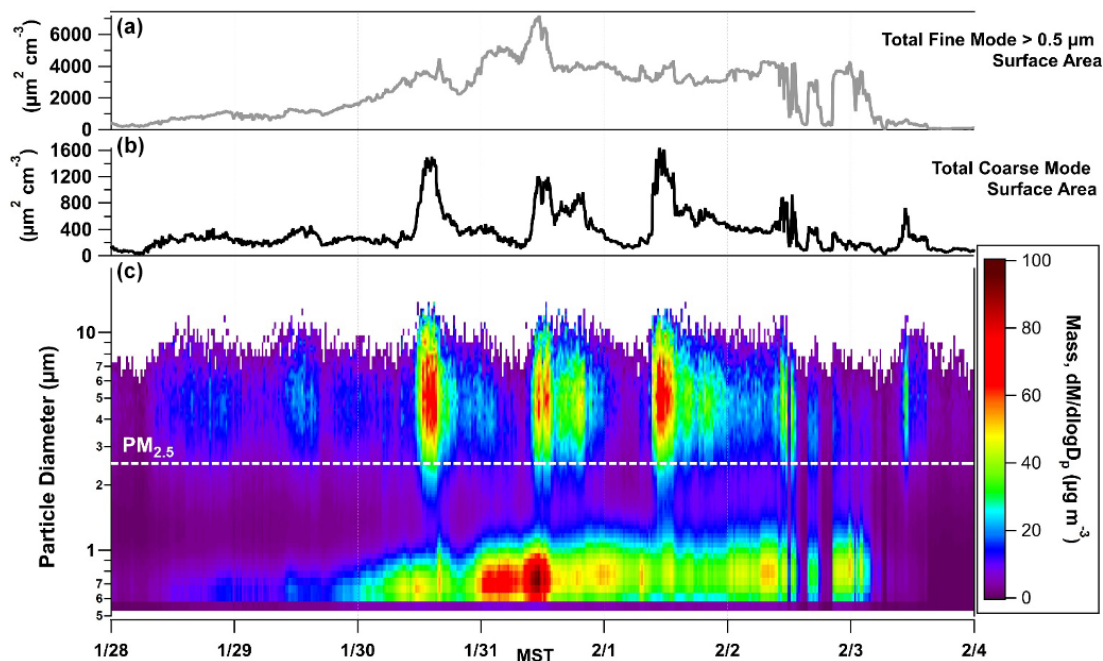
Figure 3. (a, b) The total fine-mode ($PM_{2.5}$) and coarse-mode ($> PM_{2.5}$) surface area calculated in $\mu m^2\,cm^{-3}$ from APS data. **(c)** The particle size distribution as a function of time, 28 January to 4 February, with particle size displayed along the y axis and color contours representing mass that is normalized by size bin ($dM/d\log D_p$). The population of particles that the AIM-IC captures is below the labelled $PM_{2.5}$ line.
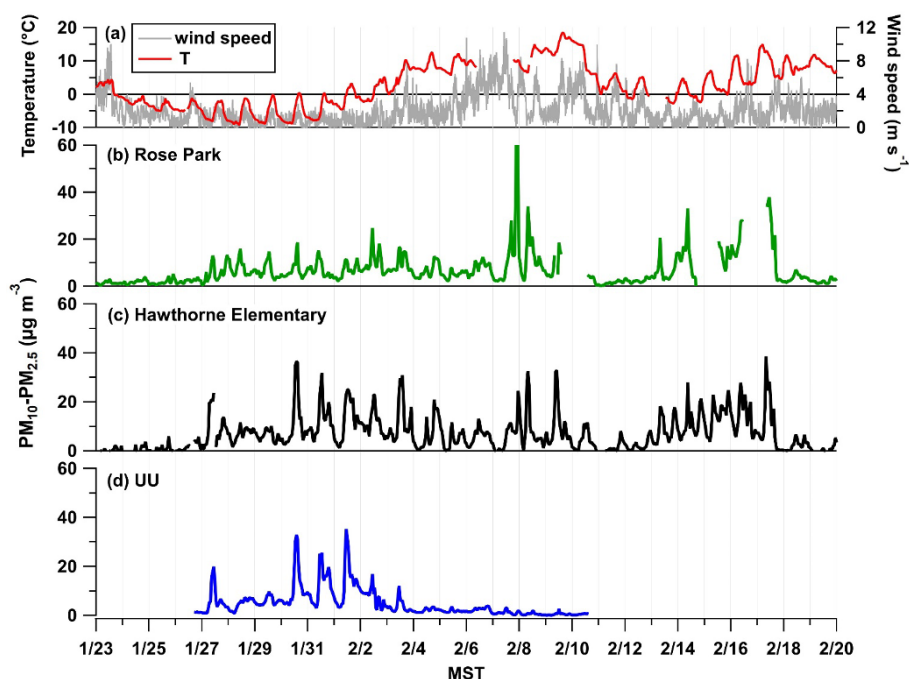

Figure 4. (a) Wind speed and temperature (°C) measured at UU. The coarse particle (PM_{10}–$PM_{2.5}$) mass loading in $\mu g\,m^{-3}$ as a function of time, 28 January to 4 February 2017, at three separate ground-based sites: Rose Park **(b)** shown in green and Hawthorne Elementary **(c)** shown in black, which are EPA monitoring sites, and the UU site **(d)** in blue.

A lower limit to the lifetime of HNO$_3$ with respect to uptake by the coarse aerosol surface can be calculated to infer the potential importance of mineral–coarse aerosol particles during these heavy pollution events. The approximate first-order removal rate of HNO$_3$ due to the heterogeneous reaction with coarse aerosols, k_{het}, depends on its average molecular speed, c; the surface area density of coarse aerosols, S_A; and the uptake coefficient, γ, given in the following expression (Ammann et al., 2013; Crowley et al., 2010; Kolb et al., 2010; Tang et al., 2017):

$$k_{het} = 0.25 \cdot c \cdot S_A \cdot \gamma. \tag{1}$$

The variation in mineralogy of coarse-mode particles can influence the efficiency in HNO$_3$ reactive uptake via the uptake coefficient, γ. This is represented in the range of reported uptake coefficients of HNO$_3$ to CaCO$_3$ ($\gamma = 0.07$ at RH $= 50$ %) and NaCl ($\gamma = 0.11$ at RH $= 55$ %) (Liu et al., 2008a; Saul et al., 2006). The average RH at peak coarse-mode loading was 54 %; therefore, the reported uptake coefficients close to this RH value were used in our calculations. Literature reports have shown RH significantly enhances the reaction probability of HNO$_3$ uptake with mineral dust and sea salts (Liu et al., 2008a; Saul et al., 2006; Vlasenko et al., 2006). The detailed kinetics of HNO$_3$ reacting with CaCO$_3$ particles in a flow reactor by Liu et al. (2008a) found low uptake values of $\gamma \leq 0.003$ at 10 % RH, while at 80 % RH, γ can be ≥ 0.21. This agrees with reports from Vlasenko et al. (2006), in which HNO$_3$ uptake on dust aerosols containing ~ 5 % CaCO$_3$ was also enhanced by an increase in RH. Saul et al. (2006) also found RH affects the uptake of HNO$_3$ onto pure NaCl showing a maximum γ of 0.12 at 50 % RH, while at 85 % RH, γ is 0.05. They also observed an increase in reactivity with the presence of MgCl$_2$ in NaCl powder. The greater reactivity of MgCl$_2$ is consistent with the hygroscopic character of magnesium salts that facilitate the increase in adsorbed water at the particle surface, which can in turn increase the effective uptake of HNO$_3$.

Because pNa$^+$ and pCa^{2+} were the dominant non-volatile species that showed common behavior with the coarse-mode mass loading, the rates of uptake with respect to NaCl and CaCO$_3$ were calculated to approximate how quickly HNO$_3$ might be sequestered. Literature values for the uptake coefficients of HNO$_3$ on NaCl (0.11 at 55 % RH) and CaCO$_3$ (0.07 at 50 % RH) were used to estimate a lifetime against reactive uptake based on the measured coarse-mode surface area (Fenter et al., 1994; Liu et al., 2008a; Vlasenko et al., 2006). The time series of k_{het} from 27 January to 4 February 2017 is presented in Fig. 5. The effective lifetime of HNO$_3$ against reactive uptake to CaCO$_3$ during episode 1 ranges from 2 to 90 min with the shortest lifetimes during periods of peak coarse-mode loading. The lifetime against NaCl (0.11) ranges from 1.3 to 57 min. These lifetime calculations assume that the entire surface is reactive and do not account for any mass transfer limitations that may occur on the particle surface. Therefore, the time range is an estimate of the

upper limit to the rate of HNO$_3$ uptake, or how quickly the reaction could potentially occur.

Under high-RH conditions, which often occur during PCAP events, it is also possible coarse particles may be deliquesced, allowing exchange between surface and bulk ions within a particle. This would result in an increased loss of nitrate if uptake were not limited to the surface. If the total mass of coarse particles measured during episode 1 were assumed to be composed of Ca(NO$_3$)$_2$, in which carbonate has been completely displaced, that would amount to an average of 6.2 µg m^{-3} of HNO$_3$ sequestered with a maximum of 32 µg m^{-3} during midday. This assumes HNO$_3$ can react with the bulk particle components, thereby representing an upper estimate of HNO$_3$ mass loss to PM$_{10}$. However, due to the size cutoff of the APS, with significant transmission losses above 10 µm, it is possible that the mass of coarse-mode particles is underestimated under some conditions.

The calculations of the removal rate do not include changes in reactive uptake associated with the changes in hygroscopicity of the resulting nitrate salts formed. The presence of calcium or magnesium nitrate salts can enhance the absorbance of water, which has been shown to increase the relative uptake of HNO$_3$ because it is no longer limited to the particle surface, so the estimation of HNO$_3$ loss can also be highly variable (Beichert and Finlayson-Pitts, 1996; Goodman et al., 2000). This is dependent on the deliquescence relative humidity (DRH) of the nitrate salt formed, in which DRH of Ca(NO$_3$)$_2$ is 10 % at 298 K (Liu et al., 2008b; Sullivan et al., 2009a, b) and NaNO$_3$ is 81 % at 273 K (Seinfeld and Pandis, 2006). The DRH is also temperature-dependent and tends to increase with decreasing temperature. The temperatures during episode 1 were consistently below 273 K; therefore, it is assumed DRH would be higher. The inference from the heterogeneous uptake calculation suggests that the loss of HNO$_3$ can be very rapid. The question of how this loss in HNO$_3$ to coarse aerosols could be shifting the gas-to-particle equilibrium that exists between HNO$_3$, NH$_3$, and NH$_4$NO$_3$ is still unknown. Therefore, further investigation of time-resolved coarse-aerosol chemical composition, in addition to PM$_{2.5}$ composition, is needed to better quantify how much coarse aerosols may be limiting HNO$_3$ availability during these PCAP pollution events and elucidate their effect on NH$_4$NO$_3$ formation.

Studies from coastal sites provide evidence that the uptake of nitrate to coarse-model aerosols can be substantial. For example, single particle measurements of sea salt particles using an aerosol time-of-flight mass spectrometer (ATOFMS) in California found that the chloride mole fraction could decrease from 0.3 to 0, while the nitrate mole fraction could increase from 0 to 0.5 following exposure of sea salt to urban air pollution (Gard et al., 1998). In coastal Florida, measurements using an online ion chromatographic technique showed that deliquesced sea salt particles could have more than 50 % of the chloride content replaced by nitrate (Dasgupta et al., 2007). Measurements from a size-resolved in-
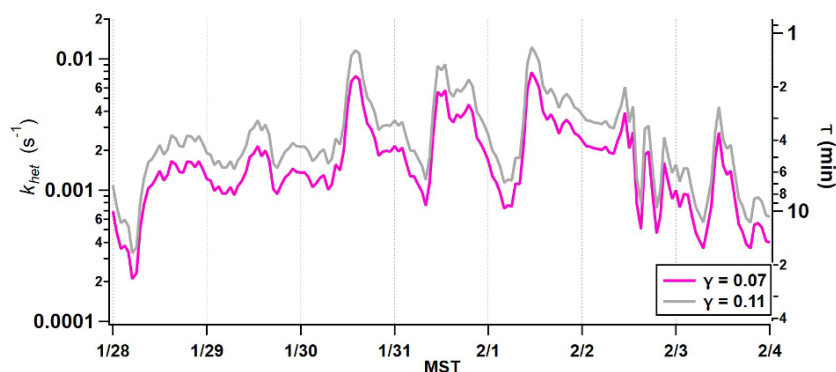
Figure 5. Predicted HNO$_3$ loss rate to coarse-particle surface area concentration measured by the APS from 28 January to 4 February 2017.

tegrated sampler showed that nitrate peaked in the coarse mode, where its concentration was close to that of chloride (on a molar basis) and half that of sodium. Size-resolved particle composition measurements near the coast in British Columbia during the summer showed that during the day, nitrate was only present in coarse-mode particles (corresponding to a deficiency in chloride), whereas during the night, nitrate could also be measured in accumulation mode particles (Anlauf et al., 2006). In addition, Lee et al. (2018) identify that coarse-mode nitrate particles, formed from acid displacement, are more important in national park areas in Arizona and Tennessee. Measurements were taken during spring and summer, respectively, so did not have competing NH$_4$NO$_3$ formation; however, they do highlight the fact coarse particle nitrate extends into the PM$_{2.5}$ regime and not all nitrate in this regime is associated with NH$_4$.

3.2.2 Evidence from snow analysis

During the campaign period, a snow event occurred prior to the first PCAP episode (21 January), in which the snow remained on the surface until 3 February. This provided a snowpack that was subjected to the first pollution event, providing a record of chemical composition changes caused by PCAP exposure. A snow event that happened later in the season occurred during clean conditions (23 February to 2 March 2017), when no PCAP was observed, thus providing a representative example of chemical composition changes in snow not associated with PCAP exposure.

Chemical analysis of the snowpack exposed to PCAP episode 1 reflects a combination of cloud water composition and the atmospheric gas and particle composition of species scavenged by snowfall or later deposited to the snow, including particles larger than the PM$_{2.5}$ cutoff monitored by the AIM-IC. Figure 6 shows a scatter plot of the NH$_4^+$ versus NO$_3^-$ measured in the snowpack, where each data point is representative of the averaged chemical composition of the entire snowpack (sampling area 0.008 m^2) on a single day, and in the atmosphere by the AIM-IC (gas phase + PM$_{2.5}$), where PM$_{2.5}$ NO$_3^-$ is assumed to be equivalent to 90 % of

PM$_{2.5}$ NH$_4^+$ on a molar basis, and by a Twin Otter aircraft (gas phase + PM$_1$). Aerosol particle measurements from the aircraft do not include non-volatile cations and their associated nitrates, which the AMS does not measure (Franchin et al., 2018). Gas-phase HNO$_3$ measurements collected on the aircraft are from the University of Washington high-resolution time-of-flight chemical ionization mass spectrometer (HR-ToF-CIMS) instrument operated similarly to the method described in Lee et al. (2018). Gas-phase NH$_3$ measurements from the Twin Otter were taken using a quantum cascade tunable infrared differential absorption spectrometer (QC-TILDAS) instrument (Aerodyne Research Inc, MA, USA) and are described in Moravek et al. (2019). Based on aircraft data (Franchin et al., 2018) and AIM-IC measurements at the ground site, the sum of nitrate in the gas phase and particle phases, or total NO$_3$ (TNO$_3$) per cubic metre of ambient air, is less than the sum of ammonia in the gas phase and particle phases, total NH$_x$ per cubic metre of ambient air. Therefore, we might expect that there would be more ammonium depositing into the snow compared to nitrate. However, in Fig. 6, it is clear that the deposition of NH$_x$ is less than half that of total NO$_3$ on a molar basis for the highest deposition amounts. The average TNO$_3$: NH$_x$ molar ratio of 3 : 1 measured in the snowpack is significantly different compared to what is observed in the atmospheric measurements. This implies that there could be another source of nitrate being deposited to the snow that is not reflected in the atmospheric measurements of the gas-phase and fine-mode particles. Therefore, there is a missing portion of the overall nitrate budget that is connected to how much NH$_4$NO$_3$ can be formed.

Further investigation into the composition of the snowpack reveals there is a strong correlation between the amount of NO$_3^-$ and the amount of Ca^{2+} ($r^2 = 0.836$), seen in Fig. 7. Both Na$^+$ and Ca^{2+} are also found in the snowpack in higher abundances than NH$_4^+$, despite being present at much lower levels in PM$_{2.5}$. The larger concentrations of pNa$^+$ relative to pCa^{2+} seen in the AIM-IC PM$_{2.5}$ data are consistent with
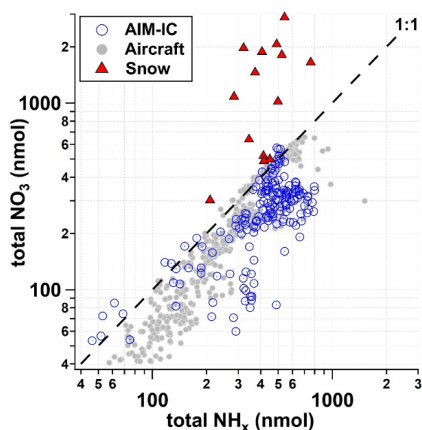
Figure 6. Total NO_3 ($pNO_3^- + HNO_3$) with respect to total NH_x measured and predicted from AIM-IC data (grey circles), aircraft measurements (open blue circles) per cubic metre of ambient air and snow (red triangles) within 0.008 m^2 sampling area from 21 January to 3 February 2017.
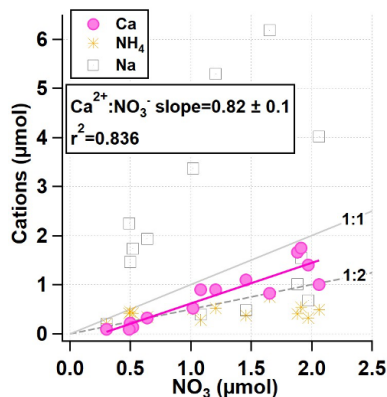

Figure 7. Daily total micromoles of NH_4, Ca, and Na vs. NO_3 within the snow from 21 January to 3 February 2017, leading into the most severe PCAP period from 27 January to 4 February 2017.

the larger concentrations of Na^+ measured in the snowpack relative to Ca^{2+} concentrations.

This suggests the coarse-mode aerosols during this PCAP event were Na-rich. Due to the large excess of micromoles of Na^+ when compared to NO_3^-, the amount of Cl^- was examined to determine whether Na-rich particles came in the form of NaCl salt. The snowpack showed the highest concentrations of Cl^- out of all of the inorganic anions measured, over 10 times more than NO_3^- and SO_4^{2-} combined. The total water-soluble ion balance measured in the snowpack shows a slight excess of anions, partially due to the high Cl^- content. However, the concentrations of Cl^- measured in the snow were greater than what can be accounted for by observed Na^+. The low concentrations of Mg^{2+} in the snowpack had no noticeable correlation with Cl^-. A closer look at the daily inorganic composition changes and decrease

in snowpack height reveals Ca^{2+} and NO_3^- exhibit similar trends throughout the lifetime of the snowpack. This is also true for changes in K^+ and Cl^- total snow column concentrations.

The proportions of non-volatile cations, where $K^+ > Na^+ > Ca^{2+} > Mg^{2+}$, found in the snow exhibit a similar distribution to that observed in $PM_{2.5}$ composition. We infer that our measurements of these constituents in $PM_{2.5}$ also reflect a larger unmeasured contribution of these non-volatile cations in the coarse mode. In addition, the nitrate present in the snow appears to have a strong correlation with Ca^{2+}, suggesting there could be a significant amount of particle nitrate in the coarse mode that is not accounted for in $PM_{2.5}$ measurements. This underestimation of particle nitrate during peak coarse-mode periods that occur during the day could lead to an underestimation in the production rate of nitrate due to photochemistry. This could impact estimates of the sensitivity of $PM_{2.5}$ to NH_3 and NO_x emissions reductions.

3.2.3 ISORROPIA analysis

The comparison of ISORROPIA model runs of predicted NH_4NO_3 ($\mu g\,m^{-3}$) with and without non-volatile components measured by the AIM-IC are depicted in Fig. 8 through pollution episode 2 from 13 to 19 February 2017 when both anion and cation gas and particle data were available. ISORROPIA calculates the equilibrium concentrations of the NH_4^+–SO_4^{2-}–NO_3^-–Na^+–Cl^-–K^+–Mg^{2+}–Ca^{2+}–H_2O system. Overall, the difference in model outputs for these two input conditions demonstrates how influential the presence of non-volatiles (pNa^+, pCa^{2+}, pMg^{2+}, and pK^+) is on the thermodynamic equilibrium between HNO_3 and its particulate counterpart pNO_3^-.

Previous studies have shown the inclusion of non-volatile cations in thermodynamic models can more accurately reproduce gas-particle partitioning observations by correctly reflecting the ion balance and the ammonium : sulfate ratio (Guo et al., 2018). With the addition of pCl^-, pNa^+, pCa^{2+}, pMg^{2+}, and pK^+ in ISORROPIA model runs, the model consistently underpredicts the concentrations of NH_4NO_3 observed. This underestimation is expected because the implicit assumption in the ISORROPIA run is that all the non-volatile cations are associated with particle nitrate, which is unlikely to be the case. The model also does not accommodate the presence of carbonate, nor does the AIM-IC measure particulate carbonate, which can also associate with non-volatile cations. Therefore, the model runs represent an upper limit of how much nitrate could be permanently trapped in the particulate phase. The model outputs imply that some non-zero fraction of the nitrate in the gas + $PM_{2.5}$ system is associated with non-volatile cations. Based on the strong relationship ISORROPIA predicts between non-volatile cations and particle nitrate, the next step is to determine how sensitive NH_4NO_3 formation is to this portion
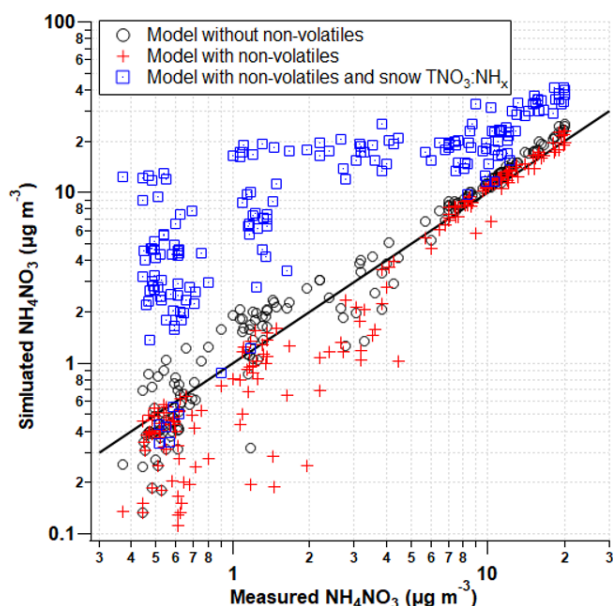
Figure 8. Predicted concentrations (ISORROPIA) with respected to measured (AIM-IC) ambient concentrations of NH$_4$NO$_3$ in µg m^{-3} through the second pollution event from 13 to 19 February 2017. The model was run in three separate conditions: (1) with (red cross) and (2) without (open black circle) the addition of pK$^+$, pCa^{2+}, and pMg^{2+} and (3) with non-volatiles and the increase in total nitrate based on the ratio of NH$_4^+$ to NO$_3^-$ measured in the snow.

of missing nitrate. Figure 8 demonstrates how much more NH$_4$NO$_3$ could be formed if HNO$_3$ was not sequestered by the coarse particles, depicted in blue squares. Based on measured gas-phase NH$_3$ and pNH$_4^+$, it is assumed there is a very little coarse-mode NH$_4^+$ in the atmosphere. To estimate the missing nitrate budget associated with coarse particles, assuming the total concentration of snow nitrate is derived from coarse particles is unrealistic. Therefore, with ambient NH$_x$ measurements as a point of reference, the total NH$_4^+$ in the snow was used to estimate the fraction of snow nitrate potentially from coarse particles, in the absence of any other direct coarse-mode measurements. The total nitrate input into ISORROPIA was calculated using the NO$_3^-$-to-NH$_4^+$ ratio observed in the snowpack during the first PCAP event. This serves as an upper limit of the missing nitrate budget and the impact this HNO$_3$ loss has on NH$_4$NO$_3$ formation. As seen in Fig. 6, the TNO$_3^-$ concentration was on average 2.5 times greater than the TNH$_4^+$ concentration measured in the snowpack. This ratio is strictly for the concentrations measured during the PCAP event. When averaging TNO$_3^-$: TNH$_4^+$ molar ratios for the full lifetime of the snowpack, the average ratio is slightly greater (3). This average ratio estimates the relative amount of TNO$_3^-$ that may come from coarse particles. This does not account for HNO$_3$ dry deposition loss; therefore, the ratio of NO$_3^-$ to NH$_4^+$ is an overestimate. However, with the combination of stable PCAP conditions, in which

the vertical mixing is suppressed, and relatively low ambient concentrations of HNO$_3$ (< 1 ppb), the dry deposition velocities would be relatively small. Therefore, this overestimate is within reason. This average molar ratio of 2.5 measured during the pollution event was applied to the total NH$_x$ measured by the AIM-IC and used as the total nitrate input into ISORROPIA along with pCl$^-$, pNa$^+$, pCa^{2+}, pMg^{2+}, and pK$^+$ concentrations observed by the AIM-IC. Overall, the model predicts greater amounts of NH$_4$NO$_3$ and, therefore, PM$_{2.5}$ will form. Based on the upper-limit estimates of the missing nitrate, the increased amounts of NH$_4$NO$_3$ modelled also represent an upper limit of how much more PM could potentially form. When observed NH$_4$NO$_3$ concentrations are above 10 µg m^{-3}, the model predicts roughly 2 times more NH$_4$NO$_3$ mass will form when nitrate lost to coarse particles is accounted for. The additional modelled pNO$_3$ mass is on average 6.8 µg m^{-3} with a maximum of 18 µg m^{-3}, which is within the upper-limit range of total nitrate loss predicted when assuming uptake to the entire bulk of the aerosol particle. This simple analysis also shows how strongly HNO$_3$-limited the PCAP event in the SLV was, when additional nitrate led to increases in NH$_4$NO$_3$. This suggests the coarse particles have the potential to control NH$_4$NO$_3$ formation indirectly by acting as a permanent sink for HNO$_3$, thereby reducing the amount of available HNO$_3$ to form PM$_{2.5}$. Therefore, future campaign studies should also include coarse particle speciation, especially in systems involving semi-volatile nitrate salts.

4   Conclusion

The AIM-IC measurements confirmed the dominance of NH$_4$NO$_3$ in wintertime PM$_{2.5}$ pollution events in the SLV. The detection of non-volatile cations (pNa$^+$, pK$^+$, pCa^{2+}, and pMg^{2+}) in PM$_{2.5}$ by the AIM-IC suggests the presence of mineral dust and/or salt during PCAP pollution events, which can potentially impact the availability of HNO$_3$. This is due to the reactive uptake of HNO$_3$ onto NaCl- and CaCO$_3$-containing particles, which can be predominantly found in the coarse mode. This can introduce a permanent sink for HNO$_3$. Due to the lack of coarse-mode speciation, auxiliary data were used to estimate the amount of HNO$_3$ potentially lost to reactive uptake. The APS surface area data were used to calculate a lifetime for HNO$_3$ with respect to uptake that was on the order of minutes, depending on the uptake coefficient used, which is influenced by particle composition (Fenter et al., 1994; Liu et al., 2008b; Vlasenko et al., 2006). The potential presence of coarse-mode nitrate was also supported by the strong correlation between total Ca^{2+} and total NO$_3^-$ observed in the snowpack. Total NO$_3^-$ in the snowpack was 2.8 times larger than the total NH$_4^+$, implying there is additional NO$_3^-$ that is not observed by PM$_{2.5}$ pNO$_3^-$ and gas-phase HNO$_3$ measurements alone.

The equilibrium dynamics were explored by thermodynamic modelling of trace gas and PM$_{2.5}$ composition, during episode 2. Despite the discrepancies between observed and modelled NH$_4$NO$_3$ concentrations during PCAP episode 2, the inclusion of coarse nitrate, from snowpack estimates, into the model shows that coarse particles could be limiting a significant portion of the HNO$_3$ being generated, preventing its reaction with NH$_3$ to form NH$_4$NO$_3$. The extent to which coarse-mode aerosols are limiting PM$_{2.5}$ formation remains unanswered and warrants further investigation of coarse-mode composition and the role these particles play in the atmospheric chemistry during pollution events.

References

Ammann, M., Cox, R. A., Crowley, J. N., Jenkin, M. E., Mellouki, A., Rossi, M. J., Troe, J., and Wallington, T. J.: Evaluated kinetic and photochemical data for atmospheric chemistry: Volume VI – heterogeneous reactions with liquid substrates, Atmos. Chem. Phys., 13, 8045–8228, https://doi.org/10.5194/acp-13-8045-2013, 2013.

Anlauf, K., Li, S. M., Leaitch, R., Brook, J., Hayden, K., Toom-Sauntry, D., and Wiebe, A.: Ionic composition and size characteristics of particles in the Lower Fraser Valley: Pacific 2001 field study, Atmos. Environ., 40, 2662–2675, https://doi.org/10.1016/j.atmosenv.2005.12.027, 2006.

Baasandorj, M., Hoch, S. W., Bares, R., Lin, J. C., Brown, S. S., Millet, D. B., Martin, R., Kelly, K., Zarzana, K. J., Whiteman, C. D., Dube, W. P., Tonnesen, G., Jaramillo, I. C., and Sohl, J.: Coupling between Chemical and Meteorological Processes under Persistent Cold-Air Pool Conditions: Evolution of Wintertime PM$_{2.5}$ Pollution Events and N2O5Observations in Utah's Salt Lake Valley, Environ. Sci. Technol., 51, 5941–5950, https://doi.org/10.1021/acs.est.6b06603, 2017.

Bares, R., Lin, J. C., Hoch, S. W., Baasandorj, M., Mendoza, D. L., Fasoli, B., Mitchell, L., Catharine, D., and Stephens, B. B.: The Wintertime Covariation of CO$_2$ and Criteria Pollutants in an Urban Valley of the Western United States, J. Geophys. Res.-Atmos., 123, 2684–2703, https://doi.org/10.1002/2017JD027917, 2018.

Behera, S. N., Sharma, M., Aneja, V. P., and Balasubramanian, R.: Ammonia in the atmosphere: A review on emission sources, atmospheric chemistry and deposition on terrestrial bodies, Environ. Sci. Pollut. Res., 20, 8092–8131, https://doi.org/10.1007/s11356-013-2051-9, 2013.

Beichert, P. and Finlayson-Pitts, B. J.: Knudsen Cell Studies of the Uptake of Gaseous HNO$_3$ and Other Oxides of Nitrogen on Solid NaCl: The Role of Surface-Adsorbed Water, J. Phys. Chem., 100, 15218–15228, https://doi.org/10.1021/jp960925u, 1996.

Bernardoni, V., Elser, M., Valli, G., Valentini, S., Bigi, A., Fermo, P., Piazzalunga, A., and Vecchi, R.: Size-segregated aerosol in a hot-spot pollution urban area: Chemical composition and three-way source apportionment, Environ. Pollut., 231, 601–611, https://doi.org/10.1016/j.envpol.2017.08.040, 2017.

Bishop, G. A., Peddle, A. M., Stedman, D. H., Air, C., Board, R., Street, I., and Box, P. O.: On-Road Emission Measurements of Reactive Nitrogen Compounds from Three California Cities, Environ. Sci. Technol., 44, 3616–3620, 2010.

Bishop, G. A., Stedman, D. H., Burgard, D. A., and Atkinson, O.: High-Mileage Light-Duty Fleet Vehicle Emissions: Their Potentially Overlooked Importance, Environ. Sci. Technol., 50, 5405–5411, https://doi.org/10.1021/acs.est.6b00717, 2016.

Chesselet, R., Morelli, J., and Buat-Menard, P.: Variations in ionic ratios between reference sea water and marine aerosols, J. Geophys. Res., 77, 5116–5131, https://doi.org/10.1029/JC077i027p05116, 1972.

Crowley, J. N., Ammann, M., Cox, R. A., Hynes, R. G., Jenkin, M. E., Mellouki, A., Rossi, M. J., Troe, J., and Wallington, T. J.: Evaluated kinetic and photochemical data for atmospheric chemistry: Volume V – heterogeneous reactions on solid substrates, Atmos. Chem. Phys., 10, 9059–9223, https://doi.org/10.5194/acp-10-9059-2010, 2010.

Dasgupta, P. K., Campbell, S. W., Al-Horr, R. S., Ullah, S. M. R., Li, J., Amalfitano, C., and Poor, N. D.: Conversion of sea salt aerosol to $NaNO_3$ and the production of HCl: Analysis of temporal behavior of aerosol chloride/nitrate and gaseous HCl/HNO_3 concentrations with AIM, Atmos. Environ., 41, 4242–4257, https://doi.org/10.1016/j.atmosenv.2006.09.054, 2007.

Fenter, F. F., Caloz, F., and Rossi, M. J.: Kinetics of nitric acid uptake by salt, J. Phys. Chem., 98, 9801–9810, https://doi.org/10.1021/j100090a014, 1994.

Fountoukis, C. and Nenes, A.: ISORROPIA II: a computationally efficient thermodynamic equilibrium model for K^+–Ca^{2+}–Mg^{2+}–NH_4^+–Na^+–SO_4^{2-}–NO_3^-–Cl^-–H_2O aerosols, Atmos. Chem. Phys., 7, 4639–4659, https://doi.org/10.5194/acp-7-4639-2007, 2007.

Franchin, A., Fibiger, D. L., Goldberger, L., McDuffie, E. E., Moravek, A., Womack, C. C., Crosman, E. T., Docherty, K. S., Dube, W. P., Hoch, S. W., Lee, B. H., Long, R., Murphy, J. G., Thornton, J. A., Brown, S. S., Baasandorj, M., and Middlebrook, A. M.: Airborne and ground-based observations of ammonium-nitrate-dominated aerosols in a shallow boundary layer during intense winter pollution episodes in northern Utah, Atmos. Chem. Phys., 18, 17259–17276, https://doi.org/10.5194/acp-18-17259-2018, 2018.

Gao, Z., Wang, X., Shen, L., Xiang, H., and Wang, H.: Observation and Source Apportionment of Trace Gases, Water-Soluble Ions and Carbonaceous Aerosol During a Haze Episode in Wuhan, Atmosphere, 10, 397, https://doi.org/10.3390/atmos10070397, 2019.

Gard, E. E., Kleeman, M. J., Gross, D. S., Hughes, L. S., Allen, J. O., Morrical, B. D., Fergenson, D. P., Dienes, T., Gälli, M. E., Johnson, R. J., Cass, G. R., and Prather, K. A.: Direct observation of heterogeneous chemistry in the atmosphere, Science, 279, 1184–1187, https://doi.org/10.1126/science.279.5354.1184, 1998.

Goodman, A. L., Underwood, G. M., and Grassian, V. H.: A laboratory study of the heterogeneous reaction of nitric acid on calcium carbonate particles, J. Geophys. Res., 105, 29053–29064, 2000.

Green, M. C., Chow, J. C., Watson, J. G., Dick, K., and Inouye, D.: Effects of snow cover and atmospheric stability on winter $PM_{2.5}$ concentrations in western U.S. Valleys, J. Appl. Meteorol. Climatol., 54, 1191–1201, https://doi.org/10.1175/JAMC-D-14-0191.1, 2015.

Guo, H., Nenes, A., and Weber, R. J.: The underappreciated role of nonvolatile cations in aerosol ammonium-sulfate molar ratios, Atmos. Chem. Phys., 18, 17307–17323, https://doi.org/10.5194/acp-18-17307-2018, 2018.

Hahnenberger, M. and Nicoll, K.: Meteorological characteristics of dust storm events in the eastern Great Basin of Utah, U.S.A., Atmos. Environ., 60, 601–612, https://doi.org/10.1016/j.atmosenv.2012.06.029, 2012.

Hansen, J. C., Woolwine, W. R., Bates, B. L., Clark, J. M., Kuprov, R. Y., Mukherjee, P., Murray, J. A., Simmons, M. A., Waite, M. F., Eatough, N. L., Eatough, D. J., Long, R., and Grover, B. D.: Semicontinuous $PM_{2.5}$ and PM_{10} mass and composition measurements in Lindon, Utah, during winter 2007, J. Air Waste Manag. Assoc., 60, 346–355, https://doi.org/10.3155/1047-3289.60.3.346, 2010.

Hansen, K., Sørensen, L. L., Hertel, O., Geels, C., Skjøth, C. A., Jensen, B., and Boegh, E.: Ammonia emissions from de-

ciduous forest after leaf fall, Biogeosciences, 10, 4577–4589, https://doi.org/10.5194/bg-10-4577-2013, 2013.

Kassomenos, P., Vardoulakis, S., Chaloulakou, A., Grivas, G., Borge, R., and Lumbreras, J.: Levels, sources and seasonality of coarse particles (PM_{10}–$PM_{2.5}$) in three European capitals – Implications for particulate pollution control, Atmos. Environ., 54, 337–347, https://doi.org/10.1016/j.atmosenv.2012.02.051, 2012.

Kelly, K. E., Kotchenruther, R., Kuprov, R., and Silcox, G. D.: Receptor model source attributions for Utah's Salt Lake City airshed and the impacts of wintertime secondary ammonium nitrate and ammonium chloride aerosol, J. Air Waste Manag. Assoc., 63, 575–590, https://doi.org/10.1080/10962247.2013.774819, 2013.

Kolb, C. E., Cox, R. A., Abbatt, J. P. D., Ammann, M., Davis, E. J., Donaldson, D. J., Garrett, B. C., George, C., Griffiths, P. T., Hanson, D. R., Kulmala, M., McFiggans, G., Pöschl, U., Riipinen, I., Rossi, M. J., Rudich, Y., Wagner, P. E., Winkler, P. M., Worsnop, D. R., and O' Dowd, C. D.: An overview of current issues in the uptake of atmospheric trace gases by aerosols and clouds, Atmos. Chem. Phys., 10, 10561–10605, https://doi.org/10.5194/acp-10-10561-2010, 2010.

Kuo, C. Y., Chen, H. H., Shih, J. F., and Wong, R. H.: Variations of nitrate and sulfate in the atmosphere on days of high and low particulate matters, Environ. Toxicol. Chem., 24, 846–851, https://doi.org/10.1897/04-198R.1, 2005.

Kuprov, R., Eatough, D. J., Cruickshank, T., Olson, N., Cropper, P. M., and Hansen, J. C.: Composition and secondary formation of fine particulate matter in the Salt Lake Valley: Winter 2009, J. Air Waste Manag. Assoc., 64, 957–969, https://doi.org/10.1080/10962247.2014.903878, 2014.

Lareau, N. P., Crosman, E., Whiteman, C. D., Horel, J. D., Hoch, S. W., Brown, W. O. J., and Horst, T. W.: The persistent cold-air pool study, Bull. Am. Meteorol. Soc., 94, 51–63, https://doi.org/10.1175/BAMS-D-11-00255.1, 2013.

Lee, B. H., Lopez-Hilfiker, F. D., Veres, P. R., McDuffie, E. E., Fibiger, D. L., Sparks, T. L., Ebben, C. J., Green, J. R., Schroder, J. C., Campuzano-Jost, P., Iyer, S., D'Ambro, E. L., Schobesberger, S., Brown, S. S., Wooldridge, P. J., Cohen, R. C., Fiddler, M. N., Bililign, S., Jimenez, J. L., Kurtén, T., Weinheimer, A. J., Jaegle, L., and Thornton, J. A.: Flight Deployment of a High-Resolution Time-of-Flight Chemical Ionization Mass Spectrometer: Observations of Reactive Halogen and Nitrogen Oxide Species, J. Geophys. Res.-Atmos., 123, 7670–7686, https://doi.org/10.1029/2017JD028082, 2018.

Li, R., Wiedinmyer, C., Baker, K. R., and Hannigan, M. P.: Characterization of coarse particulate matter in the western United States: a comparison between observation and modeling, Atmos. Chem. Phys., 13, 1311–1327, https://doi.org/10.5194/acp-13-1311-2013, 2013.

Liu, Y., Gibson, E. R., Cain, J. P., Wang, H., Grassian, V. H., and Laskin, A.: Kinetics of heterogeneous reaction of $CaCO_3$ particles with gaseous HNO_3 over a wide range of humidity, J. Phys. Chem. A, 112, 1561–1571, https://doi.org/10.1021/jp076169h, 2008a.

Liu, Y. J., Zhu, T., Zhao, D. F., and Zhang, Z. F.: Investigation of the hygroscopic properties of Ca(NO3)2 and internally mixed Ca(NO3)2 / $CaCO_3$ particles by micro-Raman spectrometry, Atmos. Chem. Phys., 8, 7205–7215, https://doi.org/10.5194/acp-8-7205-2008, 2008b.

Livingston, C., Rieger, P., and Winer, A.: Ammonia emissions from a representative in-use fleet of light and medium-duty vehicles in the California South Coast Air Basin, Atmos. Environ., 43, 3326–3333, https://doi.org/10.1016/j.atmosenv.2009.04.009, 2009.

Long, R. W., Smith, R., Smith, S., Eatough, N. L., Mangelson, N. F., Eatough, D. J., Pope, C. A., and Wilson, W. E.: Sources of fine particulate material along the wasatch front, Energ. Fuel., 16, 282–293, https://doi.org/10.1021/ef010168l, 2002.

Long, R. W., Eatough, N. L., Mangelson, N. F., Thompson, W., Fiet, K., Smith, S., Smith, R., Eatough, D. J., Pope, C. A., and Wilson, W. E.: The measurement of PM$_{2.5}$, including semi-volatile components, in the EMPACT program: results from the Salt Lake City Study, Atmos. Environ., 37, 4407–4417, https://doi.org/10.1016/s1352-2310(03)00585-5, 2003.

Malek, E., Davis, T., Martin, R. S., and Silva, P. J.: Meteorological and environmental aspects of one of the worst national air pollution episodes (January, 2004) in Logan, Cache Valley, Utah, USA, Atmos. Res., 79, 108–122, https://doi.org/10.1016/j.atmosres.2005.05.003, 2006.

Mangelson, N. F., Lewis, L., Joseph, J. M., Cui, W., Machir, J., Eatough, D. J., Rees, L. B., Wilkerson, T., and Jensen, D. T.: The contribution of sulfate and nitrate to atmospheric fine particles during winter inversion fogs in cache valley, utah, J. Air Waste Manag. Assoc., 47, 167–175, https://doi.org/10.1080/10473289.1997.10464429, 1997.

Markovic, M. Z., VandenBoer, T. C., and Murphy, J. G.: Characterization and optimization of an online system for the simultaneous measurement of atmospheric water-soluble constituents in the gas and particle phases, J. Environ. Monit., 14, 1872–84, https://doi.org/10.1039/c2em00004k, 2012.

Maxwell-Meier, K., Weber, R., Song, C., Orsini, D., Ma, Y., Carmichael, G. R., and Streets, D. G.: Inorganic composition of fine particles in mixed mineral dust-pollution plumes observed from airborne measurements during ACE-Asia, J. Geophys. Res.-Atmos., 109, 1–20, https://doi.org/10.1029/2003JD004464, 2004.

McDuffie, E. E., Womack, C. C., Fibiger, D. L., Dube, W. P., Franchin, A., Middlebrook, A. M., Goldberger, L., Lee, B. H., Thornton, J. A., Moravek, A., Murphy, J. G., Baasandorj, M., and Brown, S. S.: On the contribution of nocturnal heterogeneous reactive nitrogen chemistry to particulate matter formation during wintertime pollution events in Northern Utah, Atmos. Chem. Phys., 19, 9287–9308, https://doi.org/10.5194/acp-19-9287-2019, 2019.

Moravek, A., Murphy, J. G., Hrdina, A., Lin, J. C., Pennell, C., Franchin, A., Middlebrook, A. M., Fibiger, D. L., Womack, C. C., McDuffie, E. E., Martin, R., Moore, K., Baasandorj, M., and Brown, S. S.: Wintertime spatial distribution of ammonia and its emission sources in the Great Salt Lake region, Atmos. Chem. Phys., 19, 15691–15709, https://doi.org/10.5194/acp-19-15691-2019, 2019.

Mouteva, G. O., Randerson, J. T., Fahrni, S. M., Bush, S. E., Ehleringer, J. R., Xu, X., Santos, G. M., Kuprov, R., Schichtel, B. A., and Czimczik, C. I.: Using radiocarbon to constrain black and organic carbon aerosol sources in Salt Lake City, J. Geophys. Res.-Atmos., 122, 9843–9857, https://doi.org/10.1002/2017JD026519, 2017.

Mozurkewich, M.: The dissociation constant of ammonium nitrate and its dependence on temperature, relative humidity and particle size, Atmos. Environ. Part A, Gen. Top., 27, 261–270, https://doi.org/10.1016/0960-1686(93)90356-4, 1993.

National Oceanic and Atmospheric Administration (NOAA): Utah Winter Fine Particulate Study 2017, available at: https://csl.noaa.gov/groups/csl7/measurements/2017uwfps/ (last access: 5 October 2019), 2017.

Nenes, A., Pandis, S. N., and Pilinis, C.: ISORROPIA: A new thermodynamic equilibrium model for multiphase multicomponent inorganic aerosols, Aquat. Geoch., 4, 123–152, https://doi.org/10.1023/A:1009604003981, 1998.

Nowak, J. B., Neuman, J. A., Bahreini, R., Brock, C. A., Middlebrook, A. M., Wollny, A. G., Holloway, J. S., Peischl, J., Ryerson, T. B., and Fehsenfeld, F. C.: Airborne observations of ammonia and ammonium nitrate formation over Houston, Texas, J. Geophys. Res.-Atmos., 115, 1–12, https://doi.org/10.1029/2010JD014195, 2010.

Nowak, J. B., Neuman, J. A., Bahreini, R., Middlebrook, A. M., Holloway, J. S., McKeen, S. A., Parrish, D. D., Ryerson, T. B., and Trainer, M.: Ammonia sources in the California South Coast Air Basin and their impact on ammonium nitrate formation, Geophys. Res. Lett., 39, 6–11, https://doi.org/10.1029/2012GL051197, 2012.

Pope, C. A., Hansen, M. L., Long, R. W., Nielsen, K. R., Eatough, N. L., Wilson, W. E., and Eatough, D. J.: Ambient Particulate Air Pollution, Heart Rate Variability, and Blood Markers of Inflammation in a Panel of Elderly Subjects, Environ. Health Perspect., 112, 339–345, https://doi.org/10.1289/ehp.6588, 2003.

Pope, C. A., Krewski, D., Gapstur, S. M., Turner, M. C., Jerrett, M., and Burnett, R. T.: Fine Particulate Air Pollution and Mortality: Response to Enstrom's Reanalysis of the American Cancer Society Cancer Prevention Study II Cohort, Dose-Response, 15, 1–5, https://doi.org/10.1177/1559325817746303, 2017.

Pósfai, M., Simonics, R., Li, J., Hobbs, P. V., and Buseck, P. R.: Individual aerosol particles from biomass burning in southern Africa: 1. Compositions and size distributions of carbonaceous particles, J. Geophys. Res.-Atmos., 108, 1–13, https://doi.org/10.1029/2002jd002291, 2003.

Rissler, J., Vestin, A., Swietlicki, E., Fisch, G., Zhou, J., Artaxo, P., and Andreae, M. O.: Size distribution and hygroscopic properties of aerosol particles from dry-season biomass burning in Amazonia, Atmos. Chem. Phys., 6, 471–491, https://doi.org/10.5194/acp-6-471-2006, 2006.

Roth, P., Yang, J., Fofie, E., Cocker, D. R., Durbin, T. D., Brezny, R., Geller, M., Asa-Awuku, A., and Karavalakis, G.: Catalyzed Gasoline Particulate Filters Reduce Secondary Organic Aerosol Production from Gasoline Direct Injection Vehicles, Environ. Sci. Technol., 53, 3037–3047, https://doi.org/10.1021/acs.est.8b06418, 2019.

Saul, T. D., Tolocka, M. P., and Johnston, M. V.: Reactive uptake of nitric acid onto sodium chloride aerosols across a wide range of relative humidities, J. Phys. Chem. A, 110, 7614–7620, https://doi.org/10.1021/jp060639a, 2006.

Seinfeld, J. H. and Pandis, S. N.: Atmospheric Chemistry and Physics: From Air Pollution to Climate Change, 2nd edn., Wile-Interscience, Hoboken, New Jersey, USA, 2006.

Silcox, G. D., Kelly, K. E., Crosman, E. T., Whiteman, C. D., and Allen, B. L.: Wintertime PM$_{2.5}$ concentrations during persis-

tent, multi-day cold-air pools in a mountain valley, Atmos. Environ., 46, 17–24, https://doi.org/10.1016/j.atmosenv.2011.10.041, 2012.

Skiles, S. M. K., Mallia, D. V., Hallar, A. G., Lin, J. C., Lambert, A., Petersen, R., and Clark, S.: Implications of a shrinking Great Salt Lake for dust on snow deposition in the Wasatch Mountains, UT, as informed by a source to sink case study from the 13-14 April 2017 dust event, Environ. Res. Lett., 13, 1–9, https://doi.org/10.1088/1748-9326/aaefd8, 2018.

Suarez-Bertoa, R., Zardini, A. A., and Astorga, C.: Ammonia exhaust emissions from spark ignition vehicles over the New European Driving Cycle, Atmos. Environ., 97, 43–53, https://doi.org/10.1016/j.atmosenv.2014.07.050, 2014.

Sullivan, R. C., Moore, M. J. K., Petters, M. D., Kreidenweis, S. M., Roberts, G. C., and Prather, K. A.: Effect of chemical mixing state on the hygroscopicity and cloud nucleation properties of calcium mineral dust particles, Atmos. Chem. Phys., 9, 3303–3316, https://doi.org/10.5194/acp-9-3303-2009, 2009a.

Sullivan, R. C., Moore, M. J. K., Petters, M. D., Kreidenweis, S. M., Roberts, G. C., and Prather, K. A.: Timescale for hygroscopic conversion of calcite mineral particles through heterogeneous reaction with nitric acid, Phys. Chem. Chem. Phys., 11, 7759, https://doi.org/10.1039/b916865f, 2009b.

Sun, K., Tao, L., Miller, D. J., Pan, D., Golston, L. M., Zondlo, M. A., Griffin, R. J., Wallace, H. W., Leong, Y. J., Yang, M. M., Zhang, Y., Mauzerall, D. L., and Zhu, T.: Vehicle Emissions as an Important Urban Ammonia Source in the United States and China, Environ. Sci. Technol., 51, 2472–2481, https://doi.org/10.1021/acs.est.6b02805, 2017.

Tang, M., Huang, X., Lu, K., Ge, M., Li, Y., Cheng, P., Zhu, T., Ding, A., Zhang, Y., Gligorovski, S., Song, W., Ding, X., Bi, X., and Wang, X.: Heterogeneous reactions of mineral dust aerosol: implications for tropospheric oxidation capacity, Atmos. Chem. Phys., 17, 11727–11777, https://doi.org/10.5194/acp-17-11727-2017, 2017.

Tian, M., Liu, Y., Yang, F., Zhang, L., Peng, C., Chen, Y., Shi, G., Wang, H., Luo, B., Jiang, C., Li, B., Takeda, N., and Koizumi, K.: Increasing importance of nitrate formation for heavy aerosol pollution in two megacities in Sichuan Basin, southwest China, Environ. Pollut., 250, 898–905, https://doi.org/10.1016/j.envpol.2019.04.098, 2019.

United States Environmental Protection Agency (US EPA): NCore multipollutant monitoring network, available at: https://www3.epa.gov/ttn/amtic/ncore.html (last access: 19 November 2018), 2010.

Vecchi, R., Bernardoni, V., Valentini, S., Piazzalunga, A., Fermo, P., and Valli, G.: Assessment of light extinction at a European polluted urban area during wintertime: Impact of PM$_1$ composition and sources, Environ. Pollut., 233, 679–689, https://doi.org/10.1016/j.envpol.2017.10.059, 2018.

Vlasenko, A., Sjogren, S., Weingartner, E., Stemmler, K., Gäggeler, H. W., and Ammann, M.: Effect of humidity on nitric acid uptake to mineral dust aerosol particles, Atmos. Chem. Phys., 6, 2147–2160, https://doi.org/10.5194/acp-6-2147-2006, 2006.

Whiteman, C. D., Hoch, S. W., Horel, J. D., and Charland, A.: Relationship between particulate air pollution and meteorological variables in Utah's Salt Lake Valley, Atmos. Environ., 94, 742–753, https://doi.org/10.1016/j.atmosenv.2014.06.012, 2014.

Womack, C. C., McDuffie, E. E., Edwards, P. M., Bares, R., Gouw, J. A. A., Docherty, K. S., Dubé, W. P., Fibiger, D. L., Franchin, A., Gilman, J. B., Goldberger, L., Lee, B. H., Lin, J. C., Long, R., Middlebrook, A. M., Millet, D. B., Moravek, A., Murphy, J. G., Quinn, P. K., Riedel, T. P., Roberts, J. M., Thornton, J. A., Valin, L. C., Veres, P. R., Whitehill, A. R., Wild, R. J., Warneke, C., Yuan, B., Baasandorj, M., and Brown, S. S.: An Odd Oxygen Framework for Wintertime Ammonium Nitrate Aerosol Pollution in Urban Areas: NO$_x$ and VOC Control as Mitigation Strategies, Geophys. Res. Lett., 46, 4971–4979, https://doi.org/10.1029/2019GL082028, 2019.

Wurtsbaugh, W. A., Miller, C., Null, S. E., Justin De Rose, R., Wilcock, P., Hahnenberger, M., Howe, F., and Moore, J.: Decline of the world's saline lakes, Nat. Geosci., 10, 816–821, https://doi.org/10.1038/NGEO3052, 2017.

Zender, C. S.: Mineral Dust Entrainment and Deposition (DEAD) model: Description and 1990s dust climatology, J. Geophys. Res., 108, 1–19, https://doi.org/10.1029/2002jd002775, 2003.